

MECHANICAL AND THERMAL TRANSPORT IN NANOPOROUS GRAPHENE-LIKE BC_6N

Thi-Bao-Tien Tran^{1*}, Huu Nghia Nguyen¹,
Van Thai Nguyen²

¹ Faculty of Mechanical Engineering, Nha Trang University, Khanh Hoa, Vietnam.

² Faculty of Electrical- Electronic Engineering Technology,
Vinh Long University of Technology Education, Vinh Long, Vietnam.

Corresponding author: Thi-Bao-Tien Tran; Email: tienttb@ntu.edu.vn

Received: 17 Jan. 2024; Revised: 12 Mar. 2024; Accepted: 20 Mar. 2024

ABSTRACT

This work analyzes the thermal transport (TT) and mechanical properties (MP) of nanoporous graphene-like BC_6N monolayer utilizing non-equilibrium molecular dynamics (NEMD) and molecular dynamic (MD) simulations. Herein, the heat transfer and mechanical of nanoporous graphene-like BC_6N membrane with various circle-pore size defects are systematically reviewed and numerically examined. The results show that the BC_6N sheet has a balance on mechanical properties in two directions under biaxial tension as changing pore size from $D = 2.0$ to $D = 7.0$ nm. Young's modulus and ultimate strength of BC_6N monolayer with a circle pore decrease when the pore size increases. The trending laws are also shown to predict the mechanical parameters of the porous BC_6N sheet. Besides, the thermal conductivity (TC) of the monolayer BC_6N with a smaller pore size is much higher than that of the sample with a bigger pore size due to higher energy loss. Changing pore size can adjust the TC and 2D temperature distribution around the circle-pore. Furthermore, the pristine BC_6N TC is more heightened than the defective ones. The study results confirm that 2D- BC_6N has outstanding optical, electronic, thermal transport, and mechanical characteristics. It is particularly inspiring for further experimental and theoretical works that advance different technological applications, such as gas sensors, nanoelectronics, and optoelectronic devices. It helps for real-time monitoring, which is critical to improving safety and efficiency in marine and air transportation infrastructure.

Keywords: 2D- BC_6N , mechanical, thermal transport, energy.

I. INTRODUCTION

Graphene has attracted extensive interest as a two-dimensional (2D) material with the most stable structure of single-layer carbon atoms, exhibiting extraordinarily high thermal conductivity, mechanical strength, and exciting electronic features [1, 2]. 2D Graphene-like layered samples are formed from boron (B)–carbon (C)–nitrogen (N) atoms to create various BCN-layered materials [3]. They have been shown to have novel chemical and physical properties [4-6], which are effective for energy storage applications. Recently, a 2D-graphene-like BC_6N sheet created by an experiment-realized has attracted the special attention of many theoretical investigations based on their excellent thermal transport and mechanical properties as well as their semiconducting electronic nature [4]. Further, the layered BC_6N with a tunable band gap over

an energy-wide range offers optoelectronic and nanoelectronic device applications [5].

Nanoporosity in the atomic structure promotes phonon scattering and can substantially suppress lattice thermal conductivity, which has been theoretically confirmed [6-9]. However, there are limited studies on its intrinsic physical, mechanical, and thermal properties. Even though nanoporous 2D-carbon nitride and BC_6N structures get about three times lower TC than graphene [7-9], their rigidity is outstanding due to carbon-nitrogen bonds [10, 11], and their tensile strength can be lower compared to graphene.

Inspired by the initial studies about BC_6N , Lammmps is applied to obtain a circle pore at a graphene-like BC_6N center to create nanoporous structures with various pore sizes and estimate their mechanical and thermal characteristics. These values were analyzed

via MD simulations and NEMD calculations. Therefore, this work analyses the single-layer BC₆N mechanical properties, fracture mechanism, and thermal transport. The final results can be particularly inspiring for further experimental and theoretical studies that advance different technological applications, such as gas sensors that are used for real-time monitoring, which is critical to improving safety and efficiency in marine and air transportation infrastructure.

II. MATERIAL AND METHODS

First, under biaxial tension using MD simulations, we analyze the mechanical character of BC₆N with a circle pore defect featured by changing its radii from 2 nm to 7 nm, given in Figure 1(a). Then, we use

NEMD simulations to investigate the relation between these pore sizes versus thermal conductivity, as shown in Figure 1(b). Figure 1(a) shows the BC₆N sheet with a circle pore of 2.0/4.0/5.0/6.0/7.0 nm, corresponding to relative densities of 0.973/0.891/0.830/0.755/0.667. The BC₆N monolayer with hexagonal unicell lattice constant is about 4.98 Å [12]. The investigated BC₆N sheet has the exact dimensions of (L_x × L_y) = (11.00 × 10.50) nm. An open software, LAMMPS, is applied to conduct all NEMD and MD simulations [13, 14]. OVITO software [15] is then used to analyze the study results. The interactions of carbon-carbon atoms in graphene sheets are described by AIREBO potential [16-18] with a covalent-bonding cut-off of 2.0 Å.

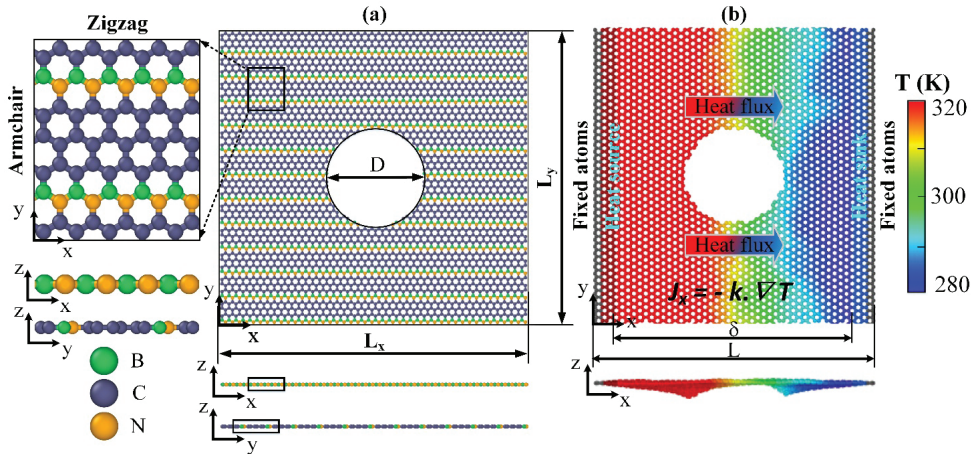


Figure 1. Simulations models of graphene-like BC₆N with variable pore sizes (a) used for biaxial tensions and (b) used for thermal transport calculations.

II. 1. Tensile process

The graphene-like BC₆N sheet undergoes an energy-minimized process by applying a conjugate-gradient program to achieve equilibrium. The Nosé-Hoover barostat and thermostat are then applied to control the pressure/temperature of the structure at 0 bar and 300 K for 300 picoseconds in the XY-plane. All directions of the model are set at periodic boundary conditions (PBC). The biaxial tensile process is performed using the deform method with the expansion of the

$$\sigma^2_{VMS} = \frac{1}{2} [6(\sigma^2_{xy} + \sigma^2_{yz} + \sigma^2_{zx}) + (\sigma_{xx} - \sigma_{yy})^2 + (\sigma_{yy} - \sigma_{zz})^2 + (\sigma_{zz} - \sigma_{xx})^2] \quad (2)$$

simulation box in both directions. It is noted that all loading processes are conducted via the NPT approach with a 0.0005 ps time step and a loading rate of 1×10⁹ s⁻¹. The formula below is used to estimate engineering strain, where L₁ and L₂ are the initial and final lengths of the BC₆N along two loading directions [19]:

$$\varepsilon = \frac{L_2 - L_1}{L_1} \quad (1)$$

The following formula is used for calculating the BC₆N von Mises stress (VMS) [20]:

where σ_{xx} , σ_{yy} , σ_{zz} are normal stresses in the x, y, and z-direction; σ_{xy} , σ_{yz} , σ_{zx} are shear strains in XY, YZ, ZX directions, respectively.

II. 2. Thermal transport calculations

For thermal transport calculations, the Steepest Descent algorithm is applied to minimize the substrate, and the system particles' initial velocity allocation is chosen by Gaussian distribution. The BC₆N sheet is relaxed at 300 K temperature using NVT and NVE methods within 500 ps and 0.0005 ps timestep, and the heat flux approach is then applied. The PBC applies on the x- and y-axis and the free boundary condition applies to the z-axis. After the equilibration stage, hot and cold slabs were set at 320 K and 280 K with a 40 K temperature difference to perform the heat flux along the x-axis for six ns to obtain the steady-state temperature gradient. The NEMD simulation model is divided into 40 slabs perpendicular to the x-axis. To keep the atom temperature at hot slabs as $T_h = T(1 + \Delta)$ K and cold slabs as $T_c = T(1 - \Delta)$ K, we applied a Langevin thermostat, in which $\Delta = 0.05$, and the averaged temperature $T = 300$ K. Separately temperature of each slab is calculated as a following formula [21],

$$T_k = \frac{1}{3n_k k_B} \sum_{i \in k} m_i v_i^2 \quad (3)$$

where n_k is atom number k in the slab k ; k_B is the Boltzmann constant; T_k is temperature; mass and velocity of atom i are v_i and m_i .

III. RESULTS AND DISCUSSION

III. 1. Mechanical properties study

This part analyzes the relation between pore size and mechanical properties of graphene-like BC₆N nanosheets under biaxial tension processes. Figure 2 shows the stress vs. strain plots in ZZ and AC directions, compared to a pristine one at ambient temperature and a strain rate of $1 \times 10^9 \text{ s}^{-1}$. The result indicates that pore defect declines the failure strength of the sample in both directions. However, its ultimate strength changes with a decreasing trend when the pore size is from 2.0 to 5.0 nm, while it increases as the pore size increases from 6.0 to 7.0 nm. These trends agree with many other nanoporous 2D materials' mechanical properties as changing pore size [19, 22].

Figure 3 shows the relationship between MPs of graphene-line BC₆N and circle pore radii. Generally, we can see a decreasing trend for four parameters, which do not depend on direction. Besides, the perfect BC₆N MPs are much higher than those of defect one. Moreover, as pore size rises from 6.0 to 7.0 nm, the toughness and failure strain slightly increase and these values also differ in two directions. It shows a similar trend to nanoporous GaSe and graphene [19, 22].

Figure 4 shows the vMs distribution of BC₆N under biaxial loading. Overall, the vMs of pore defect models are significantly smaller than those of pristine ones. We can see that the high-vMs region concentrates around the pore edge at positions perpendicular to the two opposite tensile directions. As it gets the maximum value, the atom bonds are broken,

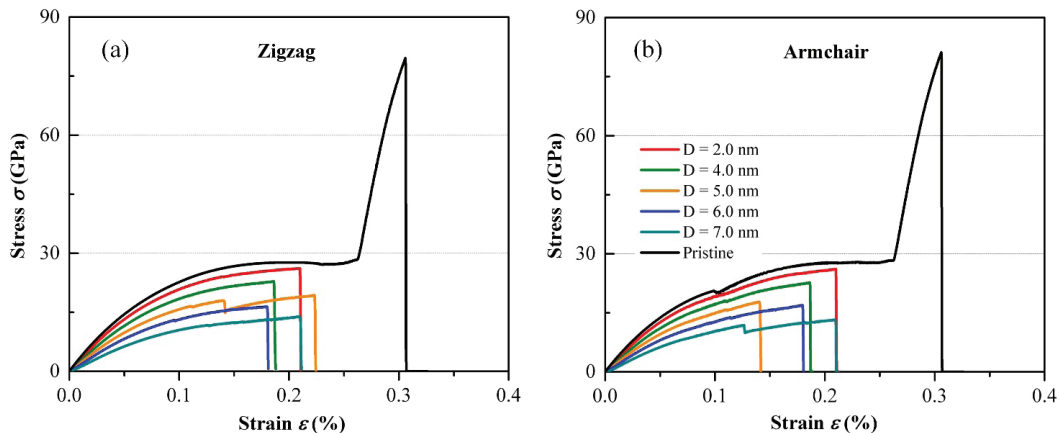


Figure 2. Stress-strain relations of graphene-like BC₆N with variable pore sizes under biaxial tension.

and fractures are formed and developed. The performed fracturing tends to create chains of BC_6N atoms around the defect circle, consistent

with a recent study [16].

Figure 5 reveals the shear strain and structural evolution of the BC_6N with various

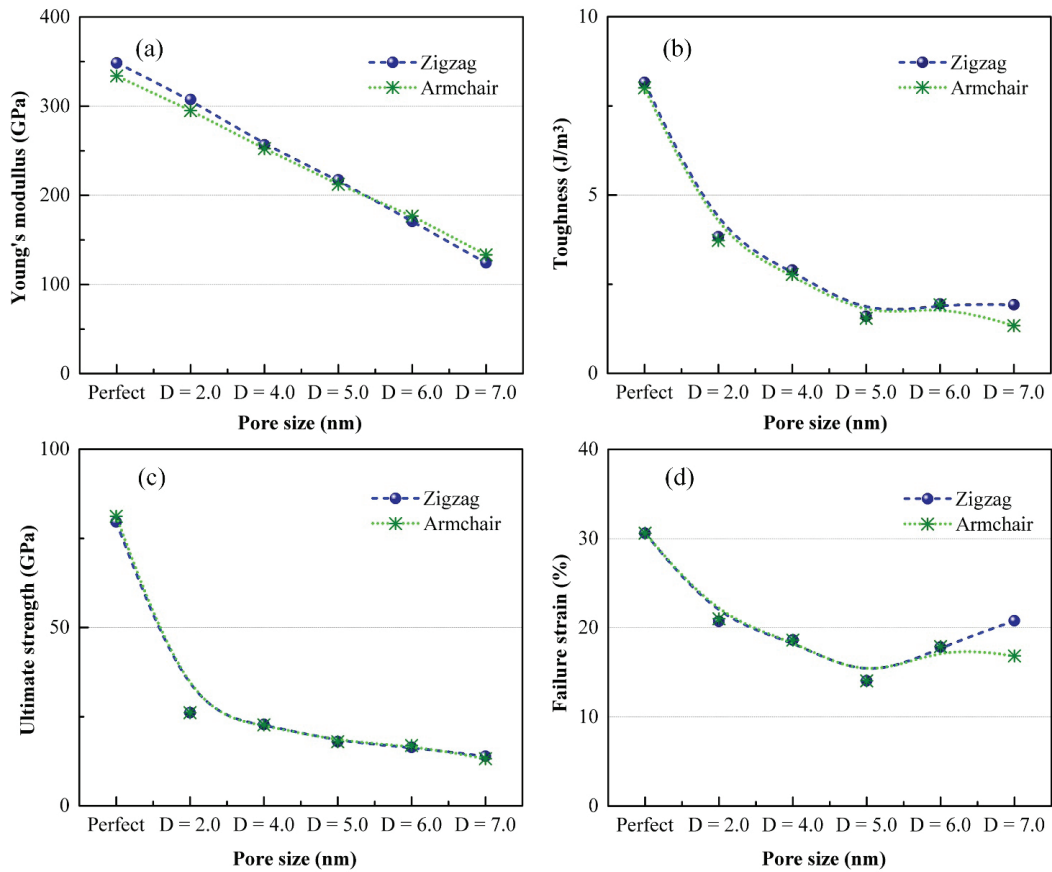


Figure 3. The mechanical parameters of graphene-like BC_6N with variable pore sizes under biaxial tension.

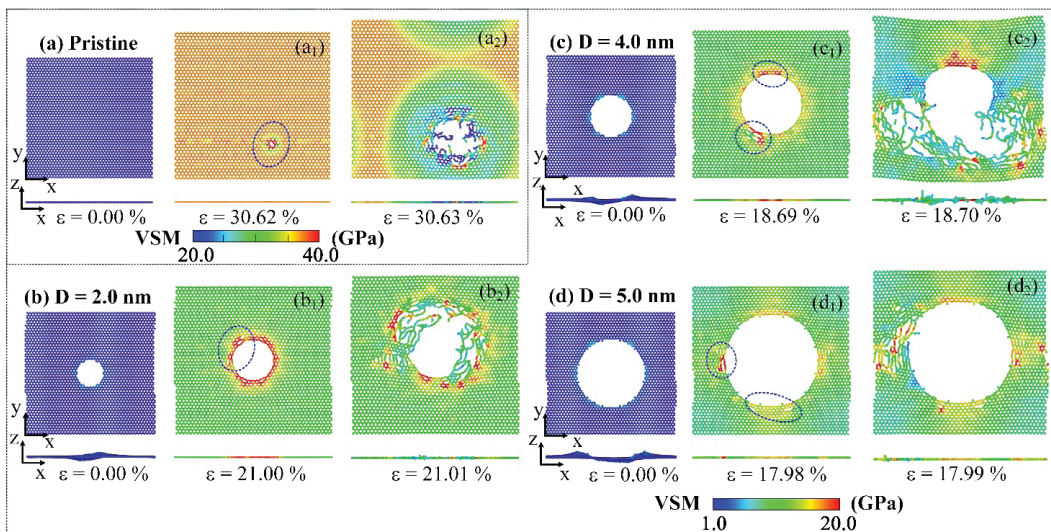


Figure 4. Von Mises stress distribution and fracture mechanism of graphene-like BC_6N with variable pore sizes during the biaxial tension.

pore radii under biaxial tension. It shows that some high shear strain area appeared on the membrane around the pore edge at the first deformation stage. The crack forming is initiated by breaking boron-carbon and boron-nitrogen bonds. The performed cracks as the strain values reach 30.62 % (for perfect model), 21% (for $D = 2\text{nm}$), 18.69% (for $D = 4\text{ nm}$), and 17.98% (for $D = 7\text{ nm}$). Furthermore, the BC_6N atoms in red correspond to the highest shear stress distributed along prolonged ruptures.

III. 2. Thermal conductivity study

Figure 6 (a-b) reveals the gained energy, dE/dT , released from and added to the hot and cold slabs along the a-axis of the sample. Herein, the sample length is 10 nm with a circle pore of 2.0 nm used for NEMD calculation at room temperature and temperature difference of 40 K. Correspondingly, Figure 6 (c-d) shows the nanoporous BC_6N temperature profiles, dT/dx , along the membrane length under two directions. Energy balance status is performed as thermal removed from the heat source equals that added to the heat sink. Herein, we set a temperature difference at 40K and an average

temperature at 300K. Heat flux is established based on the heat exchange mechanism of the hotter and the colder atoms between the heat sink and heat source, respectively. As the BC_6N sheet's temperature profile gets a steady status, the heat flux can be estimated in the x -axis through the energy line's slope [21]:

$$J_x = \frac{1}{A} \times \frac{dE}{d\tau} \quad (4)$$

where, E depicts the received energy from the thermostats, NEMD calculation time τ , and the BC_6N sheet's cross-sectional dimension A . The temperature gradient ($\partial T/\partial x$) is estimated by the temperature linear-fitting per unit slab at the steady state, shown in the sky-blue and red cut-lines of Fig. 6 (b). Therefore, TC is obtained from heat conduction Fourier law [21]:

$$k = \frac{J_x}{\partial T/\partial x} \quad (5)$$

As a result, the exchanged energy by time (dE/dT) is calculated as below formula (4). The TC of BC_6N with circle pore 2 nm can be estimated as an example, with 45.80 and 79.90 (W/mK) for the ZZ and AC orientation, consistent with others [23].

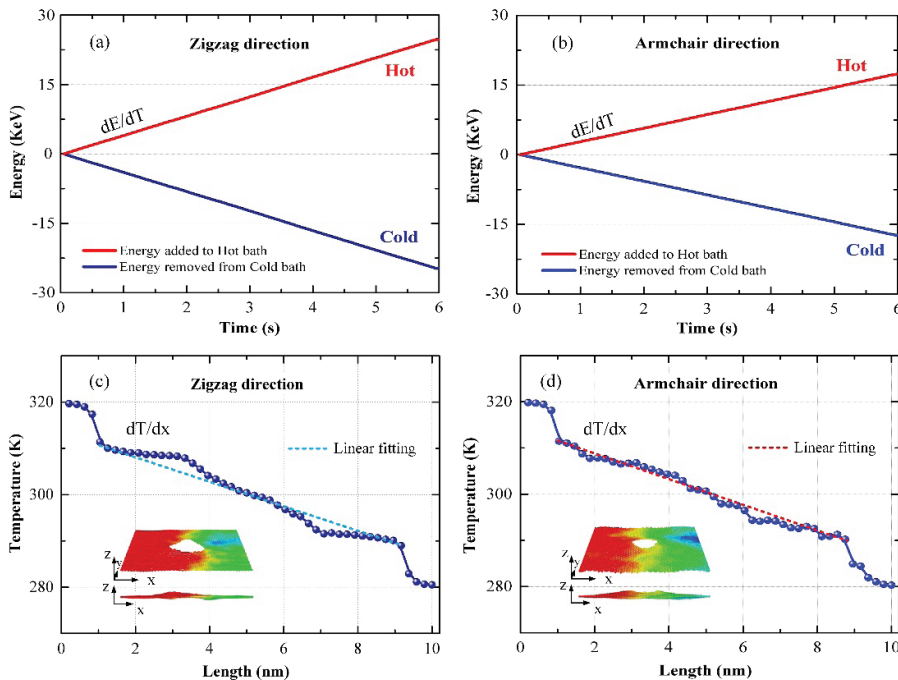


Figure 6. The exchanged energies vs. time (a-b) and temperature profile along the ZZ and AC direction (c-d) for graphene-like BC_6N with pore size $D = 2.0\text{ nm}$.

Figure 7 examines the pore defect impact BC_6N TC, performed by NEMD simulations as changing the pore size from 2.0 nm to 7.0 nm. All the samples have the same dimension of (10.0×10.0) nm². It is shown that the TC of nanoporous BC_6N is much lower than the pristine one and steadily decreases as the pore size rises. It is said that the larger the pore size,

the higher the heat flux is halted after the pore defect, resulting in a decrease in the TC due to pore orientation and elongation. Besides, these values in ZZ are higher than AC, especially for the pristine one, indicating the anisotropic in the TC of BC_6N [23]. In conclusion, the TCs of nanoporous BC_6N are sensitive to circle pore defect engineering.

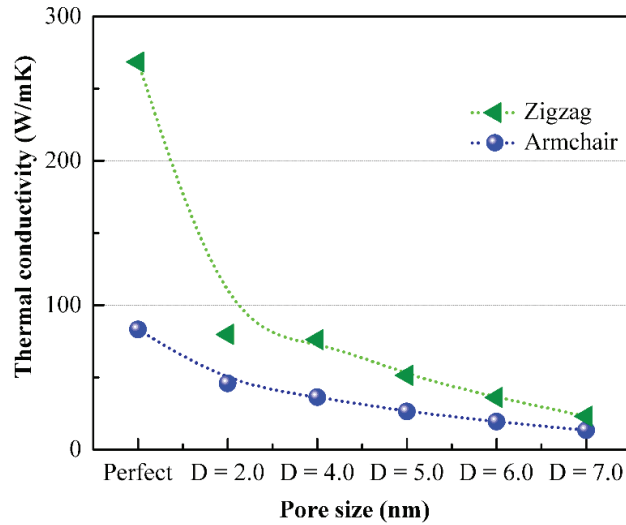


Figure 7. Nanoporous graphene-like BC_6N TC as a function of pore sizes along two directions.

Figure 8 shows 2D temperature distribution on the pristine and around the engineered circle pores of the BC_6N membranes by NEMD calculations. Herein, the temperature of fixed layers ((as shown in Figure 1(b)) of the BC_6N membranes was eliminated because these layers do not have kinetic energy. The hotter region is shown in red, and the colder region is shown in blue.

As we established, the heat transport from the hot to the cold region, from left to right of the sample length. However, the transient temperature at some positions in the center of the membranes can exceed the temperature at the heat source boundary due to the Fourier law phenomenon of 2D material, as discussed in others [21].

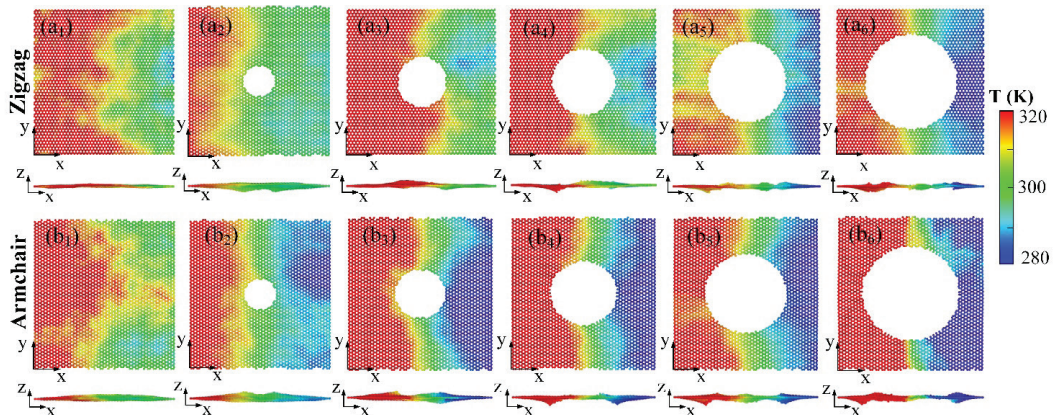


Figure 8. Temperature distribution around porous graphene-like BC_6N at ambient temperature and temperature difference $\Delta T = 40$ K.

IV. CONCLUSION

This work analyses MPs and TCs of the graphene-like BC6N sheets with various circle pore sizes using MD and NEMD calculations. We can conclude that the MP and TC of nanoporous BC6N are weakened and can be adjusted by applying the pore defect technique. Young's modulus and ultimate strength of BC6N monolayer with a circle pore decrease when the pore size increases. Besides, the thermal conductivity (TC) of the

monolayer BC6N with a smaller pore size is much higher than that of the sample with a bigger pore size due to higher energy loss. The study results confirm that 2D-BC6N has outstanding optical, electronic, thermal transport, and mechanical characteristics. It is beneficial for gas sensors, nanoelectronics, and optoelectronic applications. It helps for real-time monitoring, which is critical to improving safety and efficiency in marine and air transportation infrastructure.

REFERENCES

1. J. Y. Huang, F. Ding, B. I. Yakobson, P. Lu, L. Qi, and J. J. P. o. t. N. A. o. S. Li, "In situ observation of graphene sublimation and multi-layer edge reconstructions," vol. 106, no. 25, pp. 10103-10108, 2009.
2. A. C. Neto, F. Guinea, N. M. Peres, K. S. Novoselov, and A. K. J. R. o. m. p. Geim, "The electronic properties of graphene," vol. 81, no. 1, p. 109, 2009.
3. A. J. N. M. Rubio, "Nanoscale patchworks," vol. 9, no. 5, pp. 379-380, 2010.
4. B. J. C. Mortazavi, "Ultrahigh thermal conductivity and strength in direct-gap semiconducting graphene-like BC6N: A first-principles and classical investigation," vol. 182, pp. 373-383, 2021.
5. A. Bafekry, "Graphene-like BC6N single-layer: Tunable electronic and magnetic properties via thickness, gating, topological defects, and adatom/molecule," *Physica E: Low-dimensional Systems and Nanostructures*, vol. 118, p. 113850, 2020/04/01/ 2020.
6. S. M. Hatam-Lee, A. Rajabpour, and S. J. C. Volz, "Thermal conductivity of graphene polymorphs and compounds: From C3N to graphdiyne lattices," vol. 161, pp. 816-826, 2020.
7. B. Mortazavi, M. Makaremi, M. Shahrokhi, Z. Fan, and T. J. C. Rabczuk, "N-graphdiyne two-dimensional nanomaterials: Semiconductors with low thermal conductivity and high stretchability," vol. 137, pp. 57-67, 2018.
8. B. Mortazavi *et al.*, "Nanoporous C3N4, C3N5 and C3N6 nanosheets; novel strong semiconductors with low thermal conductivities and appealing optical/electronic properties," vol. 167, pp. 40-50, 2020.
9. S. Arabha, A. J. I. J. o. H. Rajabpour, and M. Transfer, "Thermo-mechanical properties of nitrogenated holey graphene (C2N): A comparison of machine-learning-based and classical interatomic potentials," vol. 178, p. 121589, 2021.
10. I. M. Felix and L. F. C. Pereira, "Suppression of coherent thermal transport in quasiperiodic graphene-hBN superlattice ribbons," *Carbon*, vol. 160, pp. 335-341, 2020/04/30/ 2020.
11. Y. Su, S. Cao, L.-B. Shi, and P. J. A. S. S. Qian, "Phonon-limited mobility for novel two-dimensional semiconductors of BC3 and C3N: first-principles calculation," vol. 531, p. 147341, 2020.
12. S. Demirci, N. Avazlı, E. Durgun, and S. Cahangirov, "Structural and electronic properties of monolayer group III monochalcogenides," *Physical Review B*, vol. 95, no. 11, p. 115409, 2017.
13. T.-B.-T. Tran, T.-H. Fang, V.-T. Nguyen, and V.-T. Pham, "Contact strength and deformation of straining free-standing borophene," *Computational Materials Science*, vol. 197, p. 110624, 2021/09/01/ 2021.

14. S. Plimpton, "Fast parallel algorithms for short-range molecular dynamics," *Journal of computational physics*, vol. 117, no. 1, pp. 1-19, 1995.
15. A. Stukowski, "Visualization and analysis of atomistic simulation data with OVITO—the Open Visualization Tool," *Modelling and simulation in materials science and engineering*, vol. 18, no. 1, p. 015012, 2009.
16. B. Zheng and G. X. Gu, "Tuning the graphene mechanical anisotropy via defect engineering," *Carbon*, vol. 155, pp. 697-705, 2019.
17. Z. Ding, Q.-X. Pei, J.-W. Jiang, W. Huang, and Y.-W. Zhang, "Interfacial thermal conductance in graphene/MoS₂ heterostructures," *Carbon*, vol. 96, pp. 888-896, 2016/01/01/ 2016.
18. S. J. Stuart, A. B. Tutein, and J. A. Harrison, "A reactive potential for hydrocarbons with intermolecular interactions," *The Journal of chemical physics*, vol. 112, no. 14, pp. 6472-6486, 2000.
19. T.-B.-T. Tran, T.-H. Fang, and D.-Q. Doan, "Structure-mechanical property relations of nanoporous two-dimensional gallium selenide," *Computational Materials Science*, vol. 202, p. 110985, 2022/02/01/ 2022.
20. D.-Q. Doan, T.-H. Fang, and T.-H. Chen, "Influences of grain size and temperature on tribological characteristics of CuAlNi alloys under nanoindentation and nanoscratch," *International Journal of Mechanical Sciences*, vol. 185, p. 105865, 2020/11/01/ 2020.
21. T.-B.-T. Tran, T.-H. Fang, and D.-Q. Doan, "Fracture mechanism and temperature/size-dependent thermal conductivity in gallium selenide monolayer," *Vacuum*, vol. 201, p. 111037, 2022/07/01/ 2022.
22. J. Li, C. Tian, Y. Zhang, H. Zhou, G. Hu, and R. Xia, "Structure-property relation of nanoporous graphene membranes," *Carbon*, vol. 162, pp. 392-401, 2020/06/01/ 2020.
23. H. Ghasemi, A. Rajabpour, and A. H. Akbarzadeh, "Tuning thermal conductivity of porous graphene by pore topology engineering: Comparison of non-equilibrium molecular dynamics and finite element study," *International Journal of Heat and Mass Transfer*, vol. 123, pp. 261-271, 2018/08/01/ 2018.